Academic Journal of Applied Sciences
ISSN: 3105-0549 (Print), ISSN: 3105-0557 (Online) | Vol. 1, No. 3, 2026

A Unified Framework for Epilayer Thickness Inversion Based on Lorentz–Drude Modeling and Particle Swarm Optimization

Zhixian Wang *, Mengting Ye, Bo Pang

Zhejiang Normal University, Jinhua, China

* **Corresponding author**: (Email: 15058434626@163.com)

Abstract: To address the challenge of accurately inverting epitaxial layer thickness under complex conditions, this paper proposes a comprehensive computational framework that integrates physical modeling with intelligent optimization. Methodologically, a basic model is first established based on optical interference theory, and the Lorentz–Drude composite model is introduced to characterize the frequency-dependent properties of refractive index. This approach corrects the traditional assumption of constant parameters, thereby enhancing the model's physical consistency and broadening its applicability. At the data processing level, sliding average filtering and differential screening strategies are employed to enhance the stability and noise resistance of spectral data. Furthermore, to address the nonlinear offset issues caused by multi-beam interference, a full-frequency-domain reflectance model is constructed, transforming the thickness estimation problem into a parameter optimization problem. By utilizing a particle swarm optimization algorithm for global search, the method effectively avoids the shortcomings of traditional gradient methods, such as sensitivity to initial conditions and the tendency to get stuck in local optima. Experimental results demonstrate that this method exhibits excellent stability and high accuracy under various incident conditions and across multiple datasets, significantly improving the consistency and reliability of thickness estimates. Overall, the proposed model integrates physical mechanisms with intelligent algorithms, possesses strong general applicability, and can be extended to other scenarios involving the inversion of complex optical parameters and big data modeling, thereby providing an effective analytical and optimization approach for related fields.

Keywords: Particle Swarm Optimization, Lorentz–Drude Composite Model, Multi-beam Interference Modeling.

1. Introduction

In the fields of precision manufacturing and semiconductor testing, high-precision inversion of key physical parameters is crucial for device performance evaluation and process optimization. However, in actual optical measurement processes, factors such as noise interference, non-ideal material properties, and the coupling of multiple physical effects often come into play, making it difficult for traditional analytical methods based on simplified assumptions to balance accuracy and stability. Consequently, developing an algorithmic model framework that integrates physical mechanisms with data-driven approaches has become a key research focus.

Existing methods largely rely on classical interference theory or empirical modeling, typically assuming a constant refractive index or neglecting complex effects. While effective under ideal conditions, these approaches are prone to systematic errors in practical applications. Furthermore, when addressing multi-beam interference and nonlinearity, traditional solution methods are sensitive to initial conditions and prone to getting stuck in local optima, thereby limiting the model's generalization capability. Additionally, data noise and outliers further reduce the reliability of results [1].

To address these issues, this paper proposes a unified methodological framework that integrates physical modeling with intelligent optimization. At the modeling level, frequency-dependent refractive index descriptions are introduced; at the computational level, parameter inversion is reformulated as a global optimization problem, and swarm intelligence algorithms are employed to achieve stable solutions. Concurrently, data preprocessing is utilized to enhance input quality [2][3].

Taking epitaxial layer thickness inversion as an example, this method demonstrates excellent accuracy and stability even under complex interference conditions, highlighting its strong versatility and practical value.

2. Model Construction for Thickness Inversion Based on Optical Interference and Refractive Index Modeling

2.1. Epilayer Thickness Calculation Model Based on Two-beam Interference Mechanism

The refractive indices of the epilayer and the substrate differ because of their distinct doping carrier concentrations. When infrared light is incident on the epilayer, part of the light reflects off the epilayer surface, while the rest enters the material and reflects at the interface between the epilayer and the substrate before exiting. The two reflected beams superimpose spatially to form interference, and its intensity distribution is mainly determined by the phase difference. The phase difference arises from multiple combined effects, which can generally be divided into three categories: the optical path difference caused by different propagation paths, the phase jump induced by interface reflection characteristics, and the additional phase shift due to the asymmetric refractive indices of the upper and lower interfaces.

(1) Optical Path Difference and Phase Composition

When propagating in a homogeneous medium, the optical path difference can be equivalently described by the geometric path difference. Combined with the law of refraction, the expression for the total optical path difference caused by the path difference is obtained as follows:

$$\delta = 2d_0\sqrt{n_2^2 - n_1^2 \sin^2 i_1} \tag{1}$$

Where d_0 is the thickness of the epilayer, n_1 and n_2 represent the refractive indices of the incident medium and the epilayer respectively, and i_1 is the incident angle.

In addition, extra phase changes are introduced during reflection because the media at the upper and lower interfaces of the epilayer are different. This difference can ultimately be unified as an additional phase shift term $\Delta\Phi$. Taking all factors into account, the total phase difference between the two interfering beams can be written as $\Phi = \pi - \Delta\Phi$.

(2) Expression for Epilayer Thickness

Periodic maxima or minima appear in the reflection spectrum when the optical path difference between the two reflected beams meets the interference condition. Let the interference orders corresponding to different wavelengths λ_i and λ_j be P_i and P_j respectively, then:

$$\delta_i + \frac{\lambda_i}{2} - \frac{\Delta\Phi_i\lambda_i}{2\pi} = P_i\lambda_i,\quad \delta_j + \frac{\lambda_j}{2} - \frac{\Delta\Phi_j\lambda_j}{2\pi} = (P_i + m)\lambda_j \tag{2}$$

Where m denotes the order difference between adjacent extreme points.

The refractive index is approximately independent of wavelength, so $\delta_i = \delta_j$ can be assumed. By rearranging the above equations, the expression for the interference order is obtained:

$$P_i = \frac{m\lambda_j}{\lambda_i - \lambda_j} + \frac{1}{2} - \frac{\Delta\Phi_i\lambda_i - \Delta\Phi_j\lambda_j}{2\pi(\lambda_i - \lambda_j)} \tag{3}$$

Substituting further into the interference condition formula yields the calculation formula for the epilayer thickness:

$$d_i = \left(P_i - 0.5 + \frac{\Delta\Phi_i}{2\pi}\right)\cdot\frac{\lambda_i}{\sqrt{n_2^2 - n_1^2\sin^2 i_1}} \tag{4}$$

2.2. Refractive Index Analysis Based on Lorentz-Drude Composite Model

(1) Influence of Infrared Wavelength (Lorentz Model)

When infrared electromagnetic waves are incident on a material, they couple with lattice vibrations, and this interaction is particularly strong near the optical phonon frequency. This process can usually be described by a harmonic oscillator model, which undergoes forced vibration driven by an external field with angular frequency ω.

Under this condition, the dielectric function of the material can be expressed as:

$$\varepsilon(\omega) = \varepsilon_\infty + \varepsilon_\infty\frac{\omega_{LO}^2 - \omega_{TO}^2}{\omega_{TO}^2 - \omega^2 - i\omega\Gamma} \tag{5}$$

This equation reflects the contribution of lattice vibrations to the dielectric response. Obvious dispersion occurs especially when ω is close to ω_{TO} or ω_{LO}.

(2) Influence of Carrier Concentration (Drude Model)

Besides lattice vibrations, the response of free carriers cannot be neglected. Under an applied electric field $Ee^{-i\omega t}$, electrons or holes in the conduction band can be approximately treated as free particles, whose motion is described by the Drude model.

In this model, the contribution of free carriers to the dielectric function is written as:

$$\varepsilon_p(\omega) = \varepsilon_\infty - \varepsilon_\infty\frac{\omega_p^2}{\omega^2 + i\omega\gamma_p} \tag{6}$$

Where the plasma frequency satisfies: $\omega_p^2 = \dfrac{ne^2}{4\pi^2c^2m^*\varepsilon_0\varepsilon_\infty}$.

The damping term γ_p is related to carrier mobility:

$$\gamma_p = \frac{1}{2\pi c}\cdot\frac{e}{m^*\mu} \tag{7}$$

(3) Composite Model and Refractive Index Expression

By superposing the contributions from lattice vibrations and free carriers, the complete dielectric function is obtained:

$$\varepsilon(\omega) = \varepsilon_\infty\left[1 + \frac{\omega_{LO}^2 - \omega_{TO}^2}{\omega_{TO}^2 - \omega^2 - i\omega\Gamma} - \frac{\omega_p^2}{\omega(\omega + i\gamma)}\right] \tag{8}$$

Taking its real part gives the refractive index $n = \mathrm{Re}\left\{\sqrt{\varepsilon(\omega)}\right\}$.

(4) Parameter Selection and Result Analysis

In practical calculations, 4H-SiC is adopted as the research object, and its relevant parameters are listed in Table 1. Substituting these parameters into the above model yields the curve of refractive index versus wavenumber, as shown in Figure 1.

Table 1. Parameter values for the refractive index model

Parameter	Value	Unit
ε_∞	6.52	-
ω_{TO}	793.9	cm^{-1}
ω_{TO}	970.1	cm^{-1}
Γ	4.763	cm^{-1}
m^*	0.42	-
γ	757.0	cm^{-1}

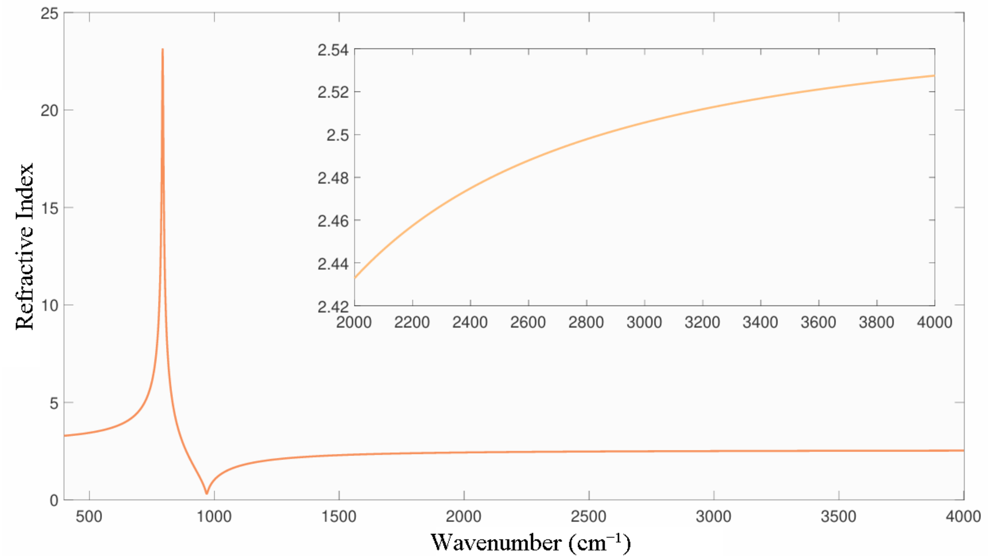

Figure 1. Schematic diagram of the relationship between wavenumber and refractive index

It can be seen from Figure 1 that the refractive index is not constant within the selected waveband, but changes noticeably with frequency. The variation becomes especially pronounced near certain frequency ranges.

2.3. Thickness Optimization Model Considering Refractive Index Variation

As the refractive index changes with wavelength, both the optical path difference and phase relations are modified accordingly, so the original model needs to be revised.

Under the condition of varying refractive index, the interference condition can be rewritten as:

$$2n_i d\sqrt{n_i^2 - n_1 \sin^2 i_1} + \frac{\lambda_i}{2} + \frac{\Delta\Phi_i}{2\pi} = P_i\lambda_i, \quad 2n_j d\sqrt{n_j^2 - n_1 \sin^2 i_1} + \frac{\lambda_j}{2} + \frac{\Delta\Phi_j}{2\pi} = (P_i + m)\lambda_j \tag{9}$$

For simplicity, the following notations are introduced: $A_i = \sqrt{n_i^2 - n_1 \sin^2 i_1}$, $A_j = \sqrt{n_j^2 - n_1 \sin^2 i_1}$.

By taking the difference of the two equations above, a corrected expression for the interference order is obtained:

$$P_i = \frac{1}{2} + \frac{\Phi_i \lambda_i A_j - \Phi_j \lambda_j A_i + 2\pi m \lambda_j A_i}{2\pi(\lambda_j A_i - \lambda_i A_j)} \tag{10}$$

It can be observed that the order is no longer determined only by the wavelength difference, but is jointly affected by refractive index variation and phase correction. Substituting this result into the thickness formula gives a corrected form for the epilayer thickness:

$$d_i = \left(\frac{\Phi_i \lambda_i A_j - \Phi_j \lambda_j A_i + 2\pi m \lambda_j A_i}{2\pi(\lambda_j A_i - \lambda_i A_j)} + \frac{\Delta\Phi_i}{2\pi} \right) \cdot \frac{\lambda_i}{\sqrt{n_i^2 - n_1 \sin^2 i_1}} \tag{11}$$

3. Robust Computation Method Based on Data Preprocessing and Difference Screening

3.1. Algorithm Design for Data Processing and Feature Extraction

(1) Data Processing

Raw spectral data usually contain obvious noise interference, and irregular fluctuations tend to appear in local regions. Therefore, five-point moving average filtering is used to denoise the spectrum.

Data quality varies significantly across different wavebands. The region below $1200\ \mathrm{cm}^{-1}$ generally lies in the strong absorption zone of the material, where interference fringes are easily suppressed or even disappear. The region above $3500\ \mathrm{cm}^{-1}$ has a low signal-to-noise ratio and is susceptible to interference from external gas absorption. Thus, only the range of $1200 \sim 3500\ \mathrm{cm}^{-1}$ is selected as the effective analysis interval.

After the above processing, a relatively smooth and continuous reflectance spectrum curve is obtained, on which peak-valley detection is performed. The processed result is shown in Figure 2. It can be seen that the interference fringes are clearly distributed and the extreme points are easy to identify.

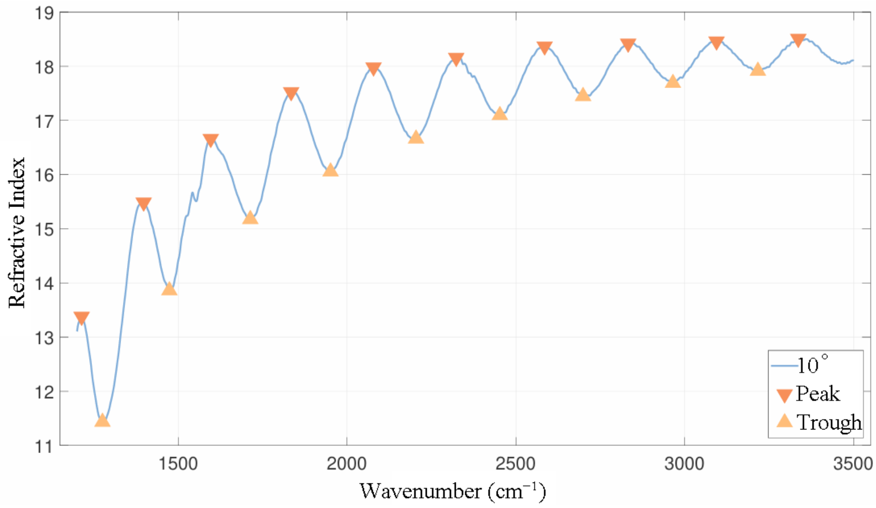

Figure 2. Schematic diagram of the relationship between wavenumber and reflectance at an incident angle of 10° after data processing

(2) Data Calculation

Based on interference theory, the order difference between adjacent extreme points should be close to 0.5. Therefore, after obtaining all p_j, difference processing is carried out:

$$\Delta p_j = p_{j+1} - p_j \tag{12}$$

By analyzing the distribution of Δp_j, abnormal points can be identified and data that do not conform to the interference law can be eliminated. Compared with directly using the original orders, the difference process is more sensitive to local errors, which helps improve the stability of the overall calculation.

(3) Result Reliability Analysis

Difference results show that the order distribution is closer to the theoretical value when refractive index variation is taken into account, indicating that model correction effectively reduces errors.

Further comparison of different model settings reveals that after introducing refractive index variation, the thickness calculation results are more concentrated with significantly reduced fluctuations. The influence of the additional phase shift term on the final result is relatively small and does not change the overall trend of thickness estimation in most cases.

Overall, the calculation strategy combining refractive index correction and difference screening can improve result stability while ensuring calculation accuracy. It also provides a foundation for subsequent modeling and optimization under multi-beam interference conditions.

3.2. Solution Results

After data processing and parameter calculation, the estimated epilayer thickness values under different incident angles can be obtained.

Specifically, when the incident angle is 10°, the calculated epilayer thickness is $7.5912\ \mu m$; when the incident angle is 15°, the corresponding thickness is $7.5001\ \mu m$. The results under the two conditions are generally close, which shows that the model has certain stability at different incident angles.

Considering fluctuations caused by a single measurement condition, the arithmetic mean of the two sets of results is taken, and the final estimated thickness is $7.5465\ \mu m$.

4. Thickness Inversion Framework Based on Multi-beam Interference and Global Optimization

4.1. Influence of Multi-Beam Interference on Epilayer Thickness Calculation

Under multi-beam interference conditions, incident light undergoes multiple reflections and transmissions inside the epilayer. The superposition of reflected beams in space forms a more complex interference structure. Compared with two-beam interference, the essential difference of this process lies in the increased number of beams participating in the superposition, which changes the final light intensity distribution [4].

Formally, the complex amplitude of multiply reflected light can be regarded as a superposition of geometric attenuation. After summation, the expression for total light intensity is obtained:

$$I = A_0^2\left[1 - \frac{(1-\rho)(1-\rho')}{1+\rho\rho' - 2\sqrt{\rho\rho'}\cos\varphi}\right] \tag{13}$$

In contrast, if only single reflection is considered, the light intensity can be simplified as:

$$I_b = A_0^2\left[\rho + \rho'(1-\rho)^2 - 2\sqrt{\rho\rho'}(1-\rho)\cos\varphi\right] \tag{14}$$

(1) Influence of Phase Offset on Thickness Calculation

In the previous model, thickness calculation relies on the constant phase difference π between adjacent interference peaks and valleys. However, this relation no longer holds strictly under multi-beam interference.

The superposition of multiply reflected light introduces extra light intensity disturbances, which shift the interference signal. This effect can be denoted as light intensity error ΔI, which further causes phase variation $\Delta\varphi$. Formally, the phase offset can be interpreted as the superposition of light intensity disturbances at each sampling point:

$$\Delta\varphi = \sum_{i=1}^{4}\frac{\partial\varphi}{\partial I_i}\Delta I_i \tag{15}$$

Further analysis shows that the phase offset is closely related to the reflectivity and the interference phase itself, and its variation is no longer constant.

It can be seen that under multi-beam interference, the phase difference corresponding to peaks and valleys has deviated from π, with a maximum offset of about 14% of one period. If uncorrected, this deviation will be directly transmitted to thickness calculation and lead to systematic errors in the results.

4.2. Solution of Epilayer Thickness for Silicon Wafer Based on Full-Frequency Domain Optimal Fitting

(1) Judgment of Multi-Beam Interference Intensity

Before solving for the thickness, it is necessary to evaluate the influence degree of multi-beam interference. Otherwise, direct application of the two-beam model usually leads to large errors. Here, the finesse F is introduced as a discriminant index to measure the sharpness of interference fringes.

Finesse is defined as the ratio of the free spectral range to the full width at half maximum:

$$\mathrm{F} = \frac{FSR}{FWHM} \tag{16}$$

Where the free spectral range corresponds to the wavelength interval between two adjacent peaks, and the full width at half maximum reflects the broadening degree of a single peak.

Under ideal two-beam interference, $\mathrm{F} \approx 2$ can be obtained. Thus, this value can be used as an empirical threshold to classify the interference type:

$\mathrm{F} < 1$: dominated by two-beam interference;

$1 < \mathrm{F} < 2$: multi-beam interference may exist;

$\mathrm{F} > 2$: multi-beam interference is significant.

It can be found from actual data that the reflectance spectrum of the given silicon wafer satisfies $\mathrm{F} > 2$ in multiple wavebands, indicating obvious multi-beam interference effects. In this case, the thickness calculation method established in the previous section based on the two-beam assumption is no longer applicable, and a new model needs to be constructed.

(2) Establishment of Reflectivity Model

Under multi-beam interference conditions, the reflected light is formed by the superposition of multiple reflections and transmissions, whose overall behavior can be described by an equivalent reflection coefficient. To simplify the problem, the incident light intensity is set to unity, and r_1, r_2 are defined as the reflection coefficients at the epilayer surface and the substrate interface respectively, while $t_1, t_{1'}$ are the corresponding transmission coefficients.

Based on the superposition relation of multiple reflections, the expression for the total reflection amplitude is obtained:

$$r = \frac{r_1 + r_2 e^{i\varphi}}{1 + r_1 r_2 e^{i\varphi}} \tag{17}$$

Where the phase difference φ can be written as:

$$\varphi = \frac{4\pi}{\lambda} n(\omega) d \cos\theta_2 + \pi - \Delta\Phi \tag{18}$$

It can be seen that the phase is related not only to the thickness d but also to the frequency-dependent refractive index $n(\omega)$. The aforementioned Lorentz-Drude model is still adopted for calculation here:

$$n(\omega) = \mathrm{Re}\left\{ \sqrt{\varepsilon_\infty \left(1 + \frac{\omega_{LO}^2 - \omega_{TO}^2}{\omega_{TO}^2 - \omega^2 - i\omega\Gamma} - \frac{\omega_p^2}{\omega(\omega + i\gamma)} \right)} \right\} \tag{19}$$

Under the assumption of no absorption, Stokes relations give $t_1 t_{1'} = 1 - r_1^2$.

Thus, the reflection amplitude expression can be further simplified to obtain the reflectivity:

$$R = \left| \frac{r_1 + r_2 e^{i\varphi}}{1 + r_1 r_2 e^{i\varphi}} \right|^2 \tag{20}$$

Where the reflection coefficients r_1, r_2 can be calculated by Fresnel equations, for example:

$$r_s = \frac{n_1(\omega)\cos\theta_1 - n_2(\omega)\cos\theta_2}{n_1(\omega)\cos\theta_1 + n_2(\omega)\cos\theta_2}, \quad r_p = \frac{n_2(\omega)\cos\theta_1 - n_1(\omega)\cos\theta_2}{n_2(\omega)\cos\theta_1 + n_1(\omega)\cos\theta_2} \tag{21}$$

(3) Solution by Particle Swarm Optimization

Under multi-beam interference, the calculation of epilayer thickness can be converted into a typical parameter fitting problem. Based on the reflectance model mentioned above, the thickness d and related physical parameters are taken as unknown variables, and a single-objective optimization model is constructed under given data constraints [5][6].

The objective function is defined as the sum of squared errors between theoretical reflectance and measured data:

$$\min \sum_i \left(\left| R(\omega_i) \right| - f(\omega_i) \right)^2 \tag{22}$$

Where $f(\omega_i)$ represents the measured reflectance at the corresponding wavenumber.

Model Establishment: To further improve fitting accuracy, the model parameters are extended to $(\gamma_1, \gamma_2, \omega_{p1}, \omega_{p2}, d)$, with constraints set within physically meaningful ranges. The optimization problem can be expressed as:

$$\min \sum_i \left(\left| R(\gamma_1, \gamma_2, \omega_{p1}, \omega_{p2}, d, \omega_i) \right| - f(\omega_i) \right)^2 \tag{23}$$

This problem is essentially a constrained nonlinear least-squares optimization problem.

Particle Swarm Optimization Strategy: The particle swarm optimization (PSO) algorithm is adopted to solve the above optimization model. This method updates individual positions and velocities continuously in the parameter space through a population search mechanism, gradually approaching the global optimal solution.

Compared with traditional gradient-based methods, PSO does not rely on derivative information and shows better adaptability to nonlinear and multimodal problems, which is particularly important for the complex reflection model in this study.

In implementation, multiple random initializations and iterative updates are used to obtain stable parameter estimates. Calculation results show that parameters converge roughly to the following ranges: $\gamma_1 \approx 28.9\ \text{cm}^{-1}$; $\gamma_2 \approx 201.7\ \text{cm}^{-1}$; $\omega_{p1} \approx 162.0\ \text{cm}^{-1}$; $\omega_{p2} \approx 750.7\ \text{cm}^{-1}$.

Fitting Results and Analysis: Substituting the optimized parameters into the reflectance model yields fitting curves over the full frequency domain, as shown in Figure 3.

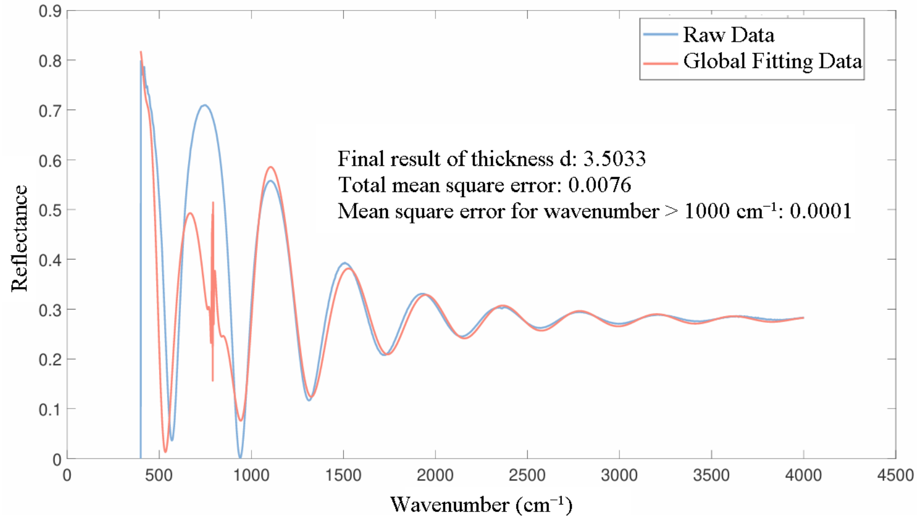

Figure 3. Full-field fitting for Dataset 3

It can be seen from the figures that the theoretical curves agree well with measured data in most spectral ranges, and the overall fitting performance is satisfactory. Further calculation of mean squared errors shows that:

Over the full spectral range, the errors are 0.0076 and 0.0104 respectively, which are generally acceptable.

When only regions with wavenumbers above $1000\ \text{cm}^{-1}$ are considered, the errors decrease significantly to the order of 10^{-4}.

This indicates that the model achieves high accuracy within the effective spectral band. Deviations in the low-wavenumber region mainly come from material absorption effects. Since the current model is based on a non-absorptive assumption, it cannot accurately describe actual optical behavior in this interval.

As shown more intuitively in Figure 3, fittings in the high-wavenumber region almost overlap completely, verifying the reliability of the model in the target band.

Result Presentation: Based on the above optimization results, the epilayer thicknesses corresponding to different datasets are obtained:

Dataset 3: $d = 3.5033\ \mu\text{m}$; Dataset 4: $d = 3.4860\ \mu\text{m}$.

The two results are close to each other, so the arithmetic mean is taken as the final estimated value: $d = 3.49465\ \mu\text{m}$.

Overall, under multi-beam interference conditions, the introduction of full-frequency-domain fitting and global optimization strategies effectively overcomes limitations of traditional methods and enables more stable and accurate thickness estimation.

5. Conclusions

This paper addresses the issue of insufficient accuracy in parameter inversion under complex interference conditions by developing an algorithmic framework that integrates physical modeling with intelligent optimization. By introducing a frequency-dependent refractive index model, the framework effectively corrects the errors caused by parameter simplification in traditional methods; combined with data filtering and differential screening strategies, it enhances the usability and stability of raw spectral data. Building on this foundation, the thickness estimation problem is reformulated as a constrained optimization problem. By employing a particle swarm optimization algorithm to perform global search, the model maintains good convergence performance even under multimodal and nonlinear conditions. Experimental results show that, under various incident angles, the estimated thickness values are concentrated within a range of approximately 7.5 µm, with fitting errors across multiple datasets as low as the 10^{-4} order of magnitude, demonstrating high accuracy and consistency. From a methodological perspective, this study has, to a certain extent, expanded the application boundaries of the integration of physical models and intelligent algorithms, offering valuable insights for complex system modeling and engineering decision-making analysis. Future research could further incorporate more real-world operating conditions and multi-source data to achieve dynamic model optimization and cross-scenario generalization.

References

[1] Wang Yang, Chen Liangfu, Li Xinxun, et al. Improvements to the Aerosol Optical Depth Inversion Algorithm for Eastern China Based on VIIRS Data [J]. Chinese Journal of Geophysics, 2019, 62(1): 49-62.

[2] Xu Yuwen, Zhang Hao, Chen Zhengchao, et al. Inversion of Aerosol Optical Thickness from Sentinel-2 Data Using the DeepBlue Algorithm [J]. Remote Sensing Technology and Applications, 2020, 35(2): 372-380.

[3] Wang Dangshe, Wang Haijiao, Zhang Miao. Parameter Selection in Thin Film Parameter Inversion Using the Particle Swarm Optimization Algorithm [J]. Journal of Xi'an University of Technology, 2011, 31(6): 518-522.

[4] Li Dong, Meng Linghui, Liu Jianxiao. A Method for Inverting Optical Parameters of High-Absorption Material Films Based

on Reflectance Spectra [J]. Laser & Optoelectronics Progress, 2025, 62(15): 1531001.

[5] Sun Yanyan, Cao Hongtao, Zhang Jiabo, et al. Remote Sensing Inversion of Water Quality Parameters Using a Support Vector Machine Model Based on Particle Swarm Optimization [J]. Science of Environmental Protection, 2025, 51(04): 86-95. DOI:10.16803/j.cnki.issn.1004-6216.202405025.

[6] Feng Zihao. A Particle Swarm Optimization-Based Method for Optimizing Centralized Control Operating Parameters in Thermal Power Plants [J]. Modern Industrial Economy and Information Technology, 2025, 15(10): 118-120. DOI: 10.16525/j.cnki.14-1362/n.2025.10.037.